Hall Mobility Measurements and Chemical Stability of Ultra Thin, Methylated Si(111)-on-Insulator Films

Jonathan E. Green, Shelley Wong and James R. Heath
Caltech Division of Chemistry and Chemical Engineering MC 127-72
1200 East California Blvd, Pasadena, CA 91125

Supplemental Information:

Detailed Experimental Methods

Impurity Doping $Si(111)_{SOI}$ wafers were diced into 1 cm^2 pieces, and the individual chips were sonicated in methanol and gently swabbed using a Texwipe CleanTip swab to remove particulates. (Note that the parent wafer was free from organic contamination since it underwent iterations of oxidation followed by BOE-etching to thin the $Si(111)_{SOI}$ epilayer.) After ensuring the wafer was free from particulates, as determined by inspection using an optical microscope at 160x magnification, a 1:10 diluted (dopant to methanol) spin-on dopant solution was spin-coated (at 4000 RPM) onto the wafer surface and subsequently baked at 200° C for 10 min to drive off excess solvent. Emulsitone (Whippany, NJ) Phosphorosilicafilm and Borosilicafilm were used for n-type and p-type doping, respectively. The dopant-film-coated wafer was then annealed under nitrogen in a rapid thermal annealer for the appropriate time and temperature to achieve a given impurity dopant concentration. The dopant film was removed by swirling the chip in BOE until the surface became hydrophobic, and surface resistivity measurements using four-point probe techniques where immediately taken. The doping was easily determined from resistivity measurements through the use of an empirical relation giving dopant density as a function of resistivity.[35,43] Dopant density vs. depth measurements were obtained by iterating four-point probe resistance measurements with CF_4-based reactive-ion etching of the Si surface to remove

approximately 5 nm at a time. A representative plot of dopant density vs. depth is shown in Figure S1 (see supporting online material).

Lithographic processing AZ-5214 (Clariant) was spin-coated onto the wafer at 4000 RPM, baked at 105° C for 5 minutes, and exposed (λ = 405 nm, area dose ≈ 20 mW/cm^2) using a Karl Suss MA-6 mask aligner through a custom-made (UCLA Nanolab mask shop, Los Angeles, CA) Cr mask. The exposed pattern was then developed in AZ-400k developer (pH ≈ 13, Clariant). The Cr mask exposed four Hall bar patterns into the photoresist (spaced by 1 mm along the perimeter of a square) and a large 2-mm square to facilitate x-ray photoelectron spectroscopy (XPS) measurements from the same chip from which the devices were fabricated. Electron-beam evaporation followed by lift-off was used to deposit 100 nm of Al onto the wafer surface to act as an etch mask. The Al Hall bar patterns were transferred into the underlying Si(111) epilayer using fluorine-based (CF_4 to He 20:30, 5 mTorr, 40 W) high-frequency reactive-ion etching (40 MHz Unaxis SLR parallel-plate RIE tool) at low substrate bias (10-20 Volts DC).

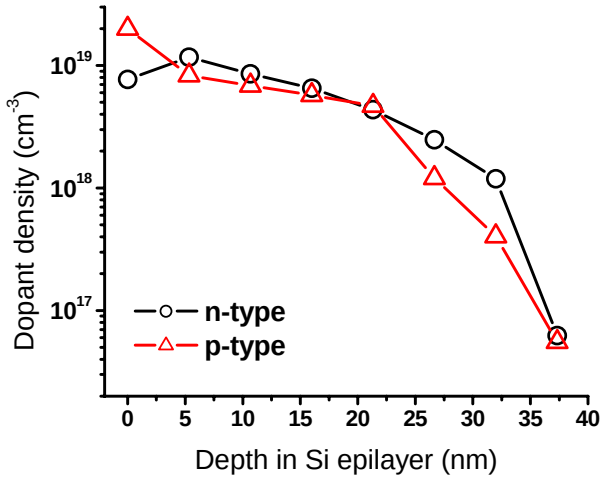

Figure S1. Dopant density vs. depth for 40-nm-thick diffusion-doped Si(111) epilayers. The n-type wafer was annealed for 5 min at 950° C; the p-type wafer was annealed for 5 min at 1050 ° C.

The endpoint was determined via interferometric detection. The Al was then removed by etching for 5 minutes in a solution of 80% H_3PO_4 + 5% HNO_3 + 5% glacial acetic acid + 10% H_2O (18 MΩ Millipore) heated to ~ 50° C, revealing four Si Hall bars and a 2-mm square sitting on top of an oxide surface. Note that devices were fabricated, as much as possible, before surface passivation. This

strategy avoided exposing the CH_3-SOI surfaces to the harsh procedures described above (particularly the AZ-400k developer, which is strongly basic, and the H_3PO_4/HNO_3 step). After methylation of the Si(111) surface, which is described in the main text, 3% PMMA or 5.5% MMA was spin-coated onto the wafer surface at 4000 RPM and subsequently baked on a hotplate heated to 180° C for 5 minutes. AZ-5214 was then spin-coated on top of the protective PMMA layer as described above. The electrical contact pattern was defined in photoresist as described above, except that a high-resolution (20,000 dots per square inch) custom-printed (Output City, Bandon Or) photomask was used instead of the Cr mask described above.

Metallization All metals were deposited using an electron-beam metal evaporator (CHA Industries Mark 40). For contact metallization, a tri-layer stack of Ti/Pt/Au (10 nm/10 nm/150 nm) was deposited at a rate of 0.25 Å s^{-1}, 0.25 Å s^{-1}, and 1 Å s^{-1}, respectively. The capping gold layer was deposited to facilitate wire bonding (see next section) using gold wire. The Pt layer was required to prevent Au from diffusing into the Si during the contact anneal, which was observed to result in a significant reduction of the device conductivity (this is not unexpected as Au impurities in Si introduce efficient mid-bandgap recombination-generation centers[16]).

Mounting to chip carrier To facilitate low-temperature Hall measurements, each device was mounted to an 8-pin Au/plastic chip carrier (model TO-100; Keystone Electronics, Astoria, NY) using rubber cement as an adhesive. Each device contact was wire-bonded to a pin on the chip carrier using Au wire and a model 747677E wire-bonding machine (West Bond Inc., Anaheim, CA).

XPS Measurements X-ray photoelectron spectroscopy (XPS) data were collected at room temperature in a UHV (10^{-9}–10^{-10} Torr) chamber described in detail elsewhere.[2, 36] X-rays from an Al Kα line (hν = 1486.6 eV) were incident to the wafer surface at

35° from the surface plane. Ejected photoelectrons were collected with a hemispherical electron energy analyzer at a take-off angle of 35° from the sample surface. Data was collected using M-probe ESCA Software version S-Probe 1.36.00. Survey scans were always taken in the energy range 0–1000 BeV (binding electron volts, or equivalently, hν minus the photoelectron energy) to confirm the presence of only Si, C, and O (except possibly Mg from the methyl-Grignard reaction). High-resolution XP spectra of the Si 2p region from approximately 97–106 BeV were used to identify any surface oxidation as indicated by the formation of a broad SiO_x peak at ~103.4 BeV. Additionally, high-resolution scans of the C 1s region from approximately 282–289 BeV were used to identify direct C–Si bonding, if possible, depending on the amount of adventitious carbon adsorbed to the surface.

Hall Measurements The Hall voltage was measured in the center of the Hall bar structure, as shown in Figure 3, to ensure the measurement is as far as possible from the end contacts of the Hall bar. The proximity of the Hall bar end contacts can cause shorting of the transverse (Hall) voltage, which leads to an underestimate of the Hall coefficient. Theoretical analysis shows that if the contacts are in the middle of the Hall bar sample, and the aspect ratio of Hall bar length (l) to width (w) is $l/w > 3$, then the error from the contacts will be less than one percent.[44] For all the Hall bar structures tested, $l/w > 7$, so edge-contact induced errors were assumed to be negligible. Perturbations to the current flow and electric field pattern caused by voltage contacts were also reduced by using monolithic contact arms and making metal-Si contact at the ends of the arms.[45]

DC Hall Measurements For most of the measurements described herein, the Hall voltage signal, V_H, was three orders of magnitude smaller than the longitudinal voltage signal, V_x. Additionally, the Hall voltage was usually offset by a 'misalignment' voltage[43] caused by a

voltage gradient parallel to the excitation current flow. This effect is usually present even in the absence of a field and for perfectly aligned Hall voltage probes. The misalignment voltage error was cancelled by measuring the Hall voltage at opposite field polarities and subtracting the two measurements. Likewise, thermoelectric and smaller magnetothermal-electric voltages (Ettingshausen and Righi-Leduc effects)[46] were eliminated by reversing the current polarity and subtracting the measured Hall voltages.

In more detail, the resistivity was measured at zero-field on opposite sides on the bar and averaged. The equations for calculating transport parameters using the DC method are as follows[46]:

Resistivity $$\rho_{1,2} = \frac{V_x(+I) - V_x(-I)}{2I}\frac{w \times t}{l} \quad , \qquad \rho_{avg} = \frac{\rho_1 + \rho_2}{2}$$

Hall factor $$R_H = \frac{\left(V_H(+B;+I) - V_H(+B;-I)\right) - \left(V_H(-B;+I) - V_H(-B;-I)\right)}{4I}\frac{t}{B}$$

Mobility $$\mu = \frac{|R_H|}{\rho_{avg}}$$

Carrier concentration $$n, p = \frac{1}{e|R_H|}$$

A constant current of 100 nA to 1 μA was used for DC measurements, and was adjusted with temperature to avoid sample heating and nonlinearities in the current-voltage response. (This was tested by doubling and/or halving the current and ensuring the voltage followed accordingly.) The applied magnetic field magnitude ranged from 3–5 T, depending on the Hall voltage signal level and the sourced current.

AC Hall measurements DC measurements from samples doped below ~4×10^{18} cm^{-3} often became unreliable at lower temperatures due to decreased signal-to-noise at the low current

levels required to avoid joule-heating.* Thus, many of the Hall measurements were made using low-frequency (≤ 13 Hz) and low current (1–10 nA) AC measurements with the measurement circuit shown in Figure 3. The advantages of the AC technique for Hall measurements are: (1) Increased signal-to-noise via synchronous detection, and (2) elimination of thermal and magnetothermal voltage offsets. However, AC measurements create their own spurious effects, which are much more difficult to diagnose than are DC measurements, due to the involvement of phase. Accordingly, AC measurements were checked where possible with DC measurements. From 100 K to 400 K, AC and DC measurements differed in most cases by less than 5%.

To eliminate the misalignment voltage, which is synchronous with the source current, V_H was calculated from the slope of V_H vs. B using two field points at each temperature. This eliminated the misalignment voltage as long as V_H was linear in B and the misalignment voltage was not field dependent. (This is also an implicit requirement for the validity of the single-carrier Drude model, upon which the transport equations used herein are based.) To that end, V_H and V_x vs. B scans were initially taken at a relatively small number of temperature points to establish the temperatures and field strengths where V_H was linear in B. Figure 4 shows typical data down to 1.75 K.

Although a rather large field of 5 T (50,000 Oe) was frequently used to increase the Hall voltage signal with respect to background (which was important for DC measurements), such fields were still within the low-field regime for the devices measured herein since the measured mobilities were generally less than 300 cm^2/V-s, giving the low-field criterion† as $B < 1/\mu \approx 1/(300\ cm^2/V\text{-}s) \approx 30$ T.

---

* Near this doping the Si:P alloy system undergoes a semiconductor-to-metal transition[49]

† The low-field criterion amounts to the requirement of non-closing cyclotron orbits. The frequency of a cyclotron orbit is $\omega_c = eB/m^*$, and an electron will be scattered before completing an orbit provided $\omega_c \langle \tau_m \rangle < 1$ radian, or $B < 1/\mu$.

The eight-contact Hall bar geometry (Figure 3) was utilized because it enabled two independent four-point longitudinal voltage measurements, V_x, and a transverse (Hall) voltage measurement, V_H, at the center of the Hall bar structure. The remaining two measurement arms were not used, but were nonetheless patterned to keep the Hall bar symmetrical. From these measurements and the known dimensions of the device, the magnetoresistivity tensor components of the thin film were calculated. This in turn enabled the calculation of the Hall mobility, μ (cm^2/V s), resistivity tensor, ρ (Ω cm), and carrier concentration, n (cm^{-3}), from the following equations[42]

$$\rho_{xx} = \rho_{yy} = 1/en\mu \qquad \text{and} \qquad \rho_{xy} = -\rho_{yx} = B/en\,. \tag{i}$$

Experimentally, a low-frequency AC or DC current was driven through the Hall bar structure and the root-mean-square (RMS) longitudinal voltage, V_x, and Hall voltage, V_H, were synchronously measured. This enabled the calculation of ρ_{xx} and ρ_{yx} from[42]

$$\rho_{xx} = \frac{E_x}{J_x} = \frac{V_x}{I}\frac{w}{l}t \qquad \text{and} \qquad \rho_{yx} = \frac{E_y}{J_x} = \frac{V_H}{I}t\,, \tag{ii}$$

where l is the distance between the same-side voltage measurement arms in Figure 3, t is the film thickness, J_x is the current density along the length of the Hall bar, and I is the current. From equations (i) and (ii), the Hall mobility and carrier density were calculated from

$$\mu = \frac{|R_H|}{\rho_{xx}} \qquad \text{and} \qquad n, p = \frac{1}{e|R_H|}; \quad R_H = \frac{t}{I}\frac{\Delta V_H}{\Delta B}\,, \tag{iii}$$

where R_H is the Hall factor (= E_y/IJ_x), and was calculated by measuring the slope of V_H as a function of the magnetic field B.

One final note, the mobility (and carrier concentration) measured using this technique is qualified with the word ‘Hall’ because it differs from the true mobility by a scattering factor. We

neglected this factor in the equations above since it is close to unity (≈ 0.95–1.2)[43] for the doping levels considered herein.